

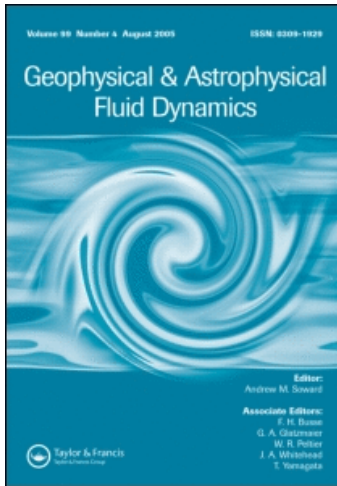
This article was downloaded by: [Keating, Shane Richard][New York University]

On: 4 March 2011

Access details: Access Details: [subscription number 933716756]

Publisher Taylor & Francis

Informa Ltd Registered in England and Wales Registered Number: 1072954 Registered office: Mortimer House, 37-41 Mortimer Street, London W1T 3JH, UK



Geophysical & Astrophysical Fluid Dynamics

Publication details, including instructions for authors and subscription information:

<http://www.informaworld.com/smpp/title~content=t713642804>

Patterns of convection in solidifying binary solutions

Shane R. Keating^a; E. A. Spiegel^b; M. G. Worster^c

^a Center for Atmosphere-Ocean Science, Courant Institute for Mathematical Sciences, New York University, New York, NY 10012, USA ^b Department of Astronomy, Columbia University, New York, NY 10027, USA ^c Institute of Theoretical Geophysics, Department of Applied Mathematics and Theoretical Physics, University of Cambridge, Cambridge CB3 0WA, UK

First published on: 04 March 2011

To cite this Article Keating, Shane R. , Spiegel, E. A. and Worster, M. G.(2011) 'Patterns of convection in solidifying binary solutions', Geophysical & Astrophysical Fluid Dynamics,, First published on: 04 March 2011 (iFirst)

To link to this Article: DOI: 10.1080/03091929.2010.545405

URL: <http://dx.doi.org/10.1080/03091929.2010.545405>

PLEASE SCROLL DOWN FOR ARTICLE

Full terms and conditions of use: <http://www.informaworld.com/terms-and-conditions-of-access.pdf>

This article may be used for research, teaching and private study purposes. Any substantial or systematic reproduction, re-distribution, re-selling, loan or sub-licensing, systematic supply or distribution in any form to anyone is expressly forbidden.

The publisher does not give any warranty express or implied or make any representation that the contents will be complete or accurate or up to date. The accuracy of any instructions, formulae and drug doses should be independently verified with primary sources. The publisher shall not be liable for any loss, actions, claims, proceedings, demand or costs or damages whatsoever or howsoever caused arising directly or indirectly in connection with or arising out of the use of this material.

Patterns of convection in solidifying binary solutions†

SHANE R. KEATING*‡, E. A. SPIEGEL§ and M. G. WORSTER¶

‡Center for Atmosphere–Ocean Science, Courant Institute for Mathematical Sciences,
New York University, 251 Mercer Street, New York, NY 10012, USA

§Department of Astronomy, Columbia University, New York, NY 10027, USA

¶Institute of Theoretical Geophysics, Department of Applied Mathematics and Theoretical
Physics, University of Cambridge, Wilberforce Road, Cambridge CB3 0WA, UK

(Received 26 January 2010; in final form 20 October 2010)

During the solidification of two-component solutions a two-phase mushy layer often forms consisting of solid dendritic crystals and solution in thermal equilibrium. Here, we extend previous weakly nonlinear analyses of convection in mushy layers to the derivation and study of a pattern equation by including a continuous spectrum of horizontal wave vectors in the development. The resulting equation is of the Swift–Hohenberg form with an additional quadratic term that destroys the up-down symmetry of the pattern as in other studies of non-Boussinesq convective pattern formation. In this case, the loss of symmetry is rooted in a non-Boussinesq dependence of the permeability on the solid-fraction of the mushy layer. We also study the motion of localized chimney structures that results from their interactions in a simplified one-dimensional approximation of the full pattern equation.

Keywords: Convection; Pattern formation; Solidification; Mushy layers; Swift–Hohenberg equation

1. Introduction

The solidification of a multi-component solution often leads to the formation of a layer of dendritic crystals in thermal equilibrium with solution in the interstices. These *mushy layers* derive from morphological instability at solidification fronts; they mediate the transition between the solid material behind an advancing solidification front and the solution ahead of it. A mushy layer is a reactive porous medium in which the solid fraction and hence the permeability evolves and so influences the dynamics of the flow within it. Mushy layers are formed in sea ice and lava lakes, at the Earth’s inner-core boundary and in other natural contexts. In industry they are formed in large alloy castings, for example. For general discussions of mushy layers and related macroscopic

*Corresponding author. Email: skeating@cims.nyu.edu

†Dedicated to Raymond “Spike” Hide, who once impressed one of us with an erudite display of little-known nondimensional numbers. Fifty-six years later, we offer him a few numbers he undoubtedly knew but did not mention.

issues in solidification theory, see Huppert (1990), Worster (1997, 2000, 2006) and Davis (2001). Weakly nonlinear analysis of the convection that typically occurs in mushy layers was carried out by Amberg and Homsy (1993) and by Anderson and Worster (1995) for geometrically simple configurations. In these treatments, discrete planforms were prescribed consisting of three superimposed rolls of different amplitude at 120° to one another. In Anderson and Worster (1995), the stability of rolls, hexagons (three rolls of equal amplitude) and mixed modes (three non-zero amplitudes, two equal) was calculated and it was concluded that there exists a transcritical bifurcation to hexagons from rolls. Anderson and Worster (1995) also detected a Hopf bifurcation from stable hexagons to an oscillatory mode, which they examined in more detail in a later paper (Anderson and Worster 1996). The oscillatory instability identified by Anderson and Worster (1996) is caused by physical interactions internal to the mush itself, in contrast to an earlier oscillatory instability studied by Chen *et al.* (1994) which owed its origin to double-diffusive convection in the solution above the mush. The theory of these oscillatory modes has been developed elsewhere (Riahi 2002, 2004, Guba and Worster 2006) and we shall discuss them no further here.

In this article, we extend the weakly nonlinear analyses of Amberg and Homsy (1993) and Anderson and Worster (1995) to the case of a continuous spectrum of horizontal wave vectors as is normally done in pattern formation analyses as developed in the context of Rayleigh–Bénard convection, for example (Manneville 1990, Cross and Hohenberg 1993). We are thereby able to retain the temporal and the horizontal spatial dependences of the planform function that would otherwise be lost by imposing *a priori* a fixed pattern of discrete rolls. Information about horizontal gradients is thus retained in the amplitude equation, and it becomes possible to study the transient spatiotemporal behaviour of the convective instability and its eventual selection of a pattern. In particular, it is shown that the horizontal planform obeys a generic pattern equation of the Swift–Hohenberg type. This result could have been anticipated based upon the rotational and reflection symmetries of the system (Cross and Hohenberg 1993); our main contribution here is a careful derivation of the relevant coefficients appearing in the pattern equations.

The second half of this article is devoted to an illustration of the utility of the spatially dependent pattern equation in solidification problems. This allows us to make a beginning on the study of the dynamics of *chimneys* — nearly vertical channels of zero solid fraction through which solute-poor liquid flows from the mush into the adjacent liquid layer (Worster 1997). These striking features of mushy layers appear as brine channels in sea ice and are believed to be responsible for “freckles” in geological formations and in alloy castings in industry, where they are mostly undesirable. From a highly simplified approximation of the full pattern equation, we can derive a dynamical system governing the motion and interactions of “nascent chimneys” (localized minima of the solid fraction) in limited circumstances. In particular, we can use this equation to examine the evolution of a (one-dimensional) lattice of widely separated chimneys and its response to defects such as the addition or removal of a chimney.

This article proceeds as follows. In section 2 we briefly review the formulation of Amberg and Homsy (1993) and Anderson and Worster (1995). In section 3 we extend the weakly nonlinear analysis of these authors to the case with a continuous spectrum of planform wave vectors to derive the relevant pattern equation, which we show to be of the Swift–Hohenberg type. We then calculate explicit expressions for the coefficients appearing in the pattern equation in terms of the physical parameters of the system for

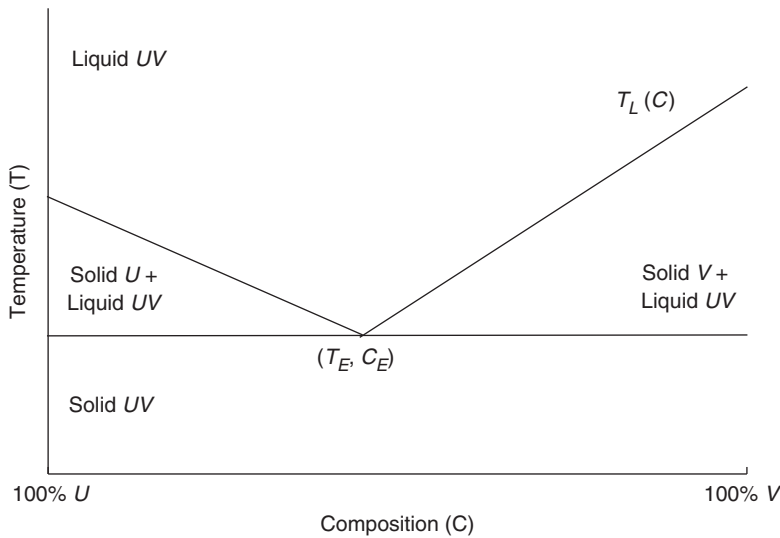


Figure 1. Simplified phase diagram for a binary solution, UV , with components U and V that exists at temperature T and composition C . Below the eutectic line, $T = T_E$, the solution is in the solid phase; above this line, at least some liquid exists. The liquidus line $T = T_L(C)$ marks the temperature at which solid U (or V) exists in thermal equilibrium with liquid UV . The lowest such temperature and the associated composition are called the eutectic temperature and composition T_E and C_E .

the near-marginal case of a narrow band of wavenumbers centred on the critical wavenumber. In section 4 we discuss the transient dynamics of widely separated interacting chimneys. Finally, we discuss our results in section 5.

2. The Model

2.1. Phenomenology

In this section we present a brief review of some of the rich phenomenology observed in solidifying binary solutions. We are interested in the upward propagation of a freezing front from below into an overlying solution UV composed of two components U and V . As indicated in the phase diagram (figure 1), a sample of the solution will be entirely liquid if the local temperature T is greater than the *liquidus* temperature $T_L(C)$, where T_L depends on the local concentration C of U in the sample. When the sample's temperature is below the *eutectic* temperature T_E , it will be solid and when $T > T_E$, at least some of the mixture will be liquid.

A transition layer, lying between the solid layer below and the purely liquid layer above, is composed of crystals of V (say) in thermodynamic equilibrium with solution UV in the interstices. As V freezes out of the solution and forms crystals, the component U is rejected, leading to an interstitial solution UV with higher relative concentration of U than in the original solution. Thus we see how the solid fraction and porosity of the transition layer and the concentration of rejected component U are dynamically coupled.

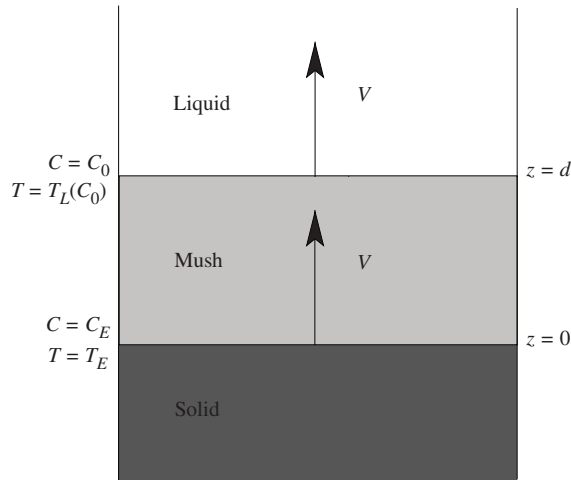


Figure 2. The model system. A solidification front advances into a binary solution at a rate V . A mushy layer of thickness d is sandwiched between a liquid and a solid region. The solid–liquid interface is at the eutectic temperature T_E ; the liquid region starts at the far-field composition C_0 and associated liquidus temperature $T_L(C_0)$.

In terms of these common observed features of the solidification of binary solutions, one may attempt to understand the propagation of a freezing front and the resulting dynamical processes. In the model of Amberg and Homsy (1993), which we adopt, the mush is modelled as a single porous layer sandwiched between liquid above and solid below (figure 2). The properties of the homogeneous material sample just described are assumed to hold *locally* throughout the system. To follow the propagation of the single porous layer at the front, we adopt Amberg and Homsy’s device of imposing comoving boundaries at the upper and lower edges of the mushy layer so as to allow us to treat the freezing process as steady in the mean, apart from the variations caused by fluid instabilities. Thus, we assume that both interfaces advance at a speed V , the mean propagation speed of the freezing front. More physically plausible boundary conditions have been considered by Chung and Chen (2000) and by Roper *et al.* (2008), with only quantitative improvement upon the work of Amberg and Homsy (1993) and Anderson and Worster (1995). Nonetheless, the formulation of Amberg and Homsy (1993), simplifies the analysis while preserving the essential physical interactions of interest and we adopt it here.

2.2. Formulation

Within the mushy layer, interstitial liquid is in thermodynamic equilibrium with fine dendritic crystals, as described in the foregoing section. Hence, within the mush, the temperature T and the concentration C are coupled via the liquidus relation

$$T = T_L(C). \quad (1)$$

We make the simplifying but qualitatively reasonable assumption that the liquidus relation (1) is approximately linear so that

$$T_L(C) = T_L(C_0) + \Gamma(C - C_0), \quad (2)$$

where Γ is the slope of the liquidus ($\Gamma > 0$ in this case). This tight coupling of the temperature and composition fields eliminates double-diffusive effects and allows us to express both T and C in terms of the single non-dimensional field

$$\theta = \frac{T - T_L(C_0)}{T_L(C_0) - T_E} = \frac{C - C_0}{C_0 - C_E}. \quad (3)$$

The quantity θ is negative within the mushy layer, rising from a value of -1 on the lower boundary to 0 at the mush–liquid interface.

The non-dimensional temperature field θ , solid fraction ϕ , fluid velocity \mathbf{u} and pressure p within the mushy layer are then governed by equations describing heat balance, solute balance, Darcy’s law for flow in a porous medium and mass continuity. The non-dimensional ideal mushy layer equations in a reference frame moving with the solidification front are given by Worster (1992, 1997) as

$$(\partial_t - \partial_z)(\theta - S\phi) + \mathbf{u} \cdot \nabla \theta = \nabla^2 \theta, \quad (4a)$$

$$(\partial_t - \partial_z)((1 - \phi)\theta + C\phi) + \mathbf{u} \cdot \nabla \theta = 0, \quad (4b)$$

$$\mathcal{K}(\phi)\mathbf{u} = -\nabla p - Ra\theta\hat{\mathbf{z}}, \quad (4c)$$

$$\nabla \cdot \mathbf{u} = 0, \quad (4d)$$

where lengths, times and velocities in (4a–d) have been scaled with κ/V , κ/V^2 and V , respectively, and κ is the thermal diffusivity. Note that, as is typical in problems of this kind, diffusion of solute is neglected in (4b). Lastly, we define

$$\mathcal{K}(\phi) = \frac{\Pi(0)}{\Pi(\phi)}, \quad (5)$$

where $\Pi(\phi)$ is the permeability as a function of solid fraction, assumed to be finite when $\phi = 0$.

The dimensionless parameters appearing in (4a–c) are the Stefan number, which gives the ratio of the latent heat to the heat available in the system,

$$S = \frac{L}{c_l(T_L(C_0) - T_E)}, \quad (6)$$

with L and c_l the latent and specific heats, respectively; the concentration ratio

$$C = \frac{C_S - C_0}{C_0 - C_E}, \quad (7)$$

which relates the difference in composition between the liquid and solid phases and the change in C across the mushy layer; and the mush Rayleigh number

$$Ra = \frac{\beta(C_0 - C_E)g\Pi(0)}{\nu V}, \quad (8)$$

where β is the linear expansion coefficient, g the acceleration due to gravity and ν the kinematic viscosity (note that the Rayleigh number is usually expressed in terms of the temperature difference across the domain rather than the concentration difference as here; however, as the temperature and concentration fields in the mushy layer are coupled via the liquidus relation, this amounts to the same thing).

A fourth dimensionless parameter,

$$\delta = \frac{Vd}{\kappa}, \quad (9)$$

can be identified as the dimensionless mush thickness and it appears in the boundary conditions

$$\theta = -1, \quad w = 0 \quad \text{on } z = 0, \quad (10a)$$

$$\theta = 0, \quad w = 0, \quad \phi = 0 \quad \text{on } z = \delta. \quad (10b)$$

These conditions correspond to impermeable rigid plates co-moving with the upper and lower boundary of the mushy layer. The lower boundary, between the solid and the mush, is maintained at the eutectic temperature T_E , while the upper boundary between the liquid and the mush (that is, at zero solid fraction ϕ), is maintained at the far-field liquidus temperature $T_L(C_0)$.

As in previous studies, we isolate the parameter regime for which there is an interesting interplay between dissolution, solidification and convection by adopting the following additional conditions. As in Amberg and Homsy (1993), we consider

$$\delta \ll 1, \quad (11)$$

which can be achieved physically by having a large far-field temperature. We make a near-eutectic approximation (Fowler 1985),

$$C = \bar{C}/\delta = O(\delta^{-1}). \quad (12)$$

We also assume a large Stefan number (Anderson and Worster 1995),

$$S = \bar{S}/\delta = O(\delta^{-1}). \quad (13)$$

The rescaled concentration ratio \bar{C} and Stefan number \bar{S} are $O(1)$ quantities.

A key implication of the near-eutectic approximation ($C = O(\delta^{-1})$) is that the solid fraction is small, hence the permeability is uniform to lowest order. Finally, following Amberg and Homsy (1993) we expand the permeability in the small solid fraction

$$\mathcal{K}(\phi) = 1 + \mathcal{K}_1\phi + \mathcal{K}_2\phi^2 + \dots \quad (14)$$

On physical grounds, one expects the permeability $\Pi(\phi)$ to be a decreasing function of solid fraction ϕ , and so \mathcal{K}_1 will be non-negative.

3. Amplitude expansion

In this section, we expand the governing equations in the spirit of Amberg and Homsy (1993) and Anderson and Worster (1995). But where these studies and those of subsequent authors treated superpositions of discrete rolls, we consider a superposition of a continuum of general planforms whose magnitudes are largest for horizontal wave-vectors in a thin annulus with radius k_c , the critical wavenumber of the linear theory, in the plane of horizontal wave vectors. By this means, we retain information about horizontal gradients in the amplitude equation, and hence need make no *a priori*

assumptions about the pattern, as in various derivations of the Swift–Hohenberg equation (Swift and Hohenberg 1977, Cross 1980, Haken 1983, Bestehorn and Haken 1983, Couillet and Spiegel 1988, Cessi *et al.* 1990).

As in Amberg and Homsy (1993) and Anderson and Worster (1995), we rescale space and time by $\mathbf{x} \rightarrow \delta \mathbf{x}$, $t \rightarrow \delta^2 t$ and $\mathbf{u} \rightarrow \delta^{-1} \mathbf{u}$, and introduce the control parameter

$$Q = \Omega \delta Ra, \quad (15)$$

where $\Omega = 1 + \bar{S}/\bar{C}$. (The control parameter Q can be identified with the quantity ΩR^2 of Anderson and Worster (1995).) We replace each dynamical field F by the sum of a stationary basic state F_B and a perturbation \hat{F} , and, for easy comparison with Anderson and Worster (1995), we adopt the following additional scalings:

$$\theta = \theta_B + \epsilon \hat{\theta}, \quad \phi = \phi_B + \epsilon \Omega^{-1} \hat{\phi}, \quad \mathbf{u} = \mathbf{0} + \epsilon \Omega^{-1} \hat{\mathbf{u}}, \quad (16a, b, c)$$

where $\mathbf{u}_B = \mathbf{0}$ and ϵ is a (small) expansion parameter to be defined below in terms of a mush Rayleigh number. The basic states $\theta_B(z)$ and $\phi_B(z)$ of the model obey

$$\delta \frac{d}{dz} \left(\theta_B - \frac{\bar{S}}{\delta} \phi_B \right) + \frac{d^2 \theta_B}{dz^2} = 0, \quad \delta \frac{d}{dz} \left((1 - \phi_B) \theta_B + \frac{\bar{C}}{\delta} \phi_B \right) = 0. \quad (17a, b)$$

Equations (17a,b) can be solved perturbatively for small δ , yielding

$$\theta_B = (z - 1) - \delta \frac{\Omega}{2} (z^2 - z) + \mathcal{O}(\delta^2), \quad \phi_B = -\frac{\delta}{\bar{C}} (z - 1) + \mathcal{O}(\delta^2). \quad (18a, b)$$

As a consequence of the near-eutectic approximation, the lowest-order contribution to the solid fraction is $\mathcal{O}(\delta)$.

Subtracting (17a,b) from the equations of motion and eliminating the pressure p via the incompressibility condition, we obtain the following equations for the perturbations θ and ϕ . On doffing hats, these become

$$(\partial_t - \delta \partial_z) \left(\Omega \theta - \frac{\bar{S}}{\delta} \phi \right) + \frac{d\theta_B}{dz} w - \Omega \nabla^2 \theta = -\epsilon \mathbf{u} \cdot \nabla \theta, \quad (19a)$$

$$(\partial_t - \delta \partial_z) \left[\left(1 - \phi_B - \epsilon \frac{\phi}{\Omega} \right) \Omega \theta + \left(\frac{\bar{C}}{\delta} - \theta_B \right) \phi \right] + \frac{d\theta_B}{dz} w = -\epsilon \mathbf{u} \cdot \nabla \theta. \quad (19b)$$

In place of (19b), we will find it convenient to use the combination (19a) $+\bar{S}/\bar{C}$ (19b), namely,

$$(\partial_t - \delta \partial_z) \left[\Omega \left(\Omega - \frac{\bar{S}}{\bar{C}} \phi_B \right) \theta - \frac{\bar{S}}{\bar{C}} (\theta_B + \epsilon \theta) \phi \right] - \Omega \nabla^2 \theta + \Omega Q \frac{d\theta_B}{dz} w = -\epsilon \Omega Q \mathbf{u} \cdot \nabla \theta. \quad (19c)$$

In addition to (19a,c), we have the equations for the perturbations \mathbf{u} , which can be written in the concise form

$$\nabla^2 (\mathcal{K}(\phi) \mathbf{u}) - \nabla (\mathbf{u} \cdot \nabla \mathcal{K}) - Q \nabla \times \nabla \times \theta \hat{\mathbf{z}} = 0, \quad (20)$$

where $\hat{\mathbf{z}}$ is the unit vector in the vertical direction.

The boundary conditions are

$$\theta = w = 0 \quad \text{on } z = 0, \quad (21a)$$

$$\theta = w = \phi = 0 \quad \text{on } z = 1. \quad (21b)$$

In principle, u , v and w can be eliminated from (19a,c) by using the diagnostic equation (20); in practice, it is easier to write (19a,c), (20) schematically in the form of a single prognostic equation

$$(\mathcal{L} + \mathcal{T}\partial_t)\mathbf{v} = \epsilon\mathbf{N}, \quad (22)$$

where $\mathbf{v} = \{\phi, \theta, \mathbf{u}\}$ is the vector of perturbed fields, $\mathcal{L} + \mathcal{T}\partial_t$ is the linear operator, and $\epsilon\mathbf{N}$ are the nonlinearities. Explicit expressions for the linear operators \mathcal{L} and \mathcal{T} and the nonlinearity \mathbf{N} can be found in appendix A.

Equation (22) can then be solved perturbatively by expanding each of the fields in powers of ϵ as

$$\mathbf{v} = \mathbf{v}_0 + \epsilon\mathbf{v}_1 + \epsilon^2\mathbf{v}_2 + \dots \quad (23)$$

Likewise, we expand the control parameter Q , and, therefore, the linear operator \mathcal{L} as

$$Q = Q_0 + \epsilon Q_1 + \epsilon^2 Q_2 + \dots, \quad \mathcal{L} = \mathcal{L}_0 + \epsilon\mathcal{L}_1 + \epsilon^2\mathcal{L}_2 \dots \quad (24a, b)$$

The operator \mathcal{T} is $\mathcal{O}(\epsilon^0)$.

At higher orders in ϵ , (22) yields a system of linear inhomogeneous differential equations, so that we can look for solutions of the form

$$\mathbf{v}_n(\mathbf{x}, z, t, T) = \int d\mathbf{k} d\sigma e^{i\mathbf{k}\cdot\mathbf{x} + \sigma t} \tilde{\mathbf{v}}_{n,\sigma\mathbf{k}}(z, T), \quad (25)$$

where $T = \epsilon^2 t$ is the slow time scale on which the amplitudes vary, $\mathbf{k} = (k_x, k_y)$ and $\mathbf{x} = (x, y)$.

In addition, we separate the lowest-order solution so that

$$\tilde{\mathbf{v}}_{0,\sigma\mathbf{k}} = \begin{pmatrix} \tilde{\phi}_{0,\sigma\mathbf{k}} \\ \tilde{\theta}_{0,\sigma\mathbf{k}} \\ \tilde{w}_{0,\sigma\mathbf{k}} \end{pmatrix} = \begin{pmatrix} \Phi_{0,\sigma\mathbf{k}}(z) \\ \Theta_{0,\sigma\mathbf{k}}(z) \\ W_{0,\sigma\mathbf{k}}(z) \end{pmatrix} \tilde{f}_{\sigma\mathbf{k}}(T), \quad (26)$$

where $\tilde{f}_{\sigma\mathbf{k}}(T)$ is the Fourier–Laplace transform of the planform function $f(\mathbf{x}, t, T)$. In (26), the number of dynamical variables has been reduced to three using the incompressibility condition, which gives expressions for the two horizontal components of velocity in terms of the vertical component:

$$\tilde{u}_{0,\sigma\mathbf{k}} = i \frac{k_x}{k^2} W'_{0,\sigma\mathbf{k}} \tilde{f}_{\sigma\mathbf{k}}(T), \quad \tilde{v}_{0,\sigma\mathbf{k}} = i \frac{k_y}{k^2} W'_{0,\sigma\mathbf{k}} \tilde{f}_{\sigma\mathbf{k}}(T), \quad (27a, b)$$

where primes denote differentiation with respect to z .

Following Anderson and Worster (1995), at each order in ϵ we expand in powers of δ ; that is, we perform an asymptotic expansion in the ordered limit $\epsilon \ll \delta \ll 1$. This yields

$$\mathbf{v} = (\mathbf{v}_{00} + \delta\mathbf{v}_{01} + \dots) + \epsilon(\mathbf{v}_{10} + \delta\mathbf{v}_{11} + \dots) + \epsilon^2(\delta^{-1}\mathbf{v}_{2,-1} + \mathbf{v}_{20} + \dots) + \dots, \quad (28a)$$

$$Q = (Q_{00} + \delta Q_{01} + \dots) + \epsilon(Q_{10} + \delta Q_{11} + \dots) + \epsilon^2(Q_{20} + \delta Q_{21} + \dots) + \dots, \quad (28b)$$

$$\sigma = (\sigma_{00} + \delta\sigma_{01} + \dots) + \epsilon(\sigma_{10} + \delta\sigma_{11} + \dots) + \epsilon^2(\sigma_{20} + \delta\sigma_{21} + \dots) + \dots, \quad (28c)$$

where, because \mathcal{S} , $\mathcal{C} = \mathcal{O}(\delta^{-1})$, we must include in the expansion the field $\mathbf{v}_{2,-1} = \{\phi_{2,-1}, 0, \mathbf{0}\}$.

3.1. Linear analysis

At the lowest order, $O(\epsilon^0\delta^{-1})$, we obtain

$$\sigma_0\Phi_{00,\sigma\mathbf{k}} = 0, \tag{29}$$

implying that $\sigma\Phi_{0,\sigma\mathbf{k}} = O(\delta)$.

At $O(\epsilon^0\delta^0)$, we find solutions

$$\Theta_{00,\sigma\mathbf{k}} = -\sin(\pi z), \quad W_{00,\sigma\mathbf{k}} = (\pi^2 + k^2)\sqrt{1 + \frac{\Omega\sigma_0}{\pi^2 + k^2}} \sin(\pi z), \tag{30a,b}$$

along with the associated solutions for $\tilde{u}_{00,\sigma\mathbf{k}}$ and $\tilde{v}_{00,\sigma\mathbf{k}}$ given by (27a,b).

In addition to the solutions (30a,b), we seek the linear perturbation to the solid fraction $\Phi_{0,\sigma\mathbf{k}}$. However, (29) requires that we consider terms of higher order in δ . Anderson and Worster (1996) showed that, for the case of $\sigma = O(\delta)$, $\Phi_{0,\sigma\mathbf{k}} = O(1)$, the dispersion relation admits complex solutions, indicating the presence of an oscillatory instability. As we are interested in the parameter regime near the marginal stability curve $Q = Q_{00}(k) + O(\epsilon)$ in the asymptotic limit $\epsilon \ll \delta \ll 1$, we will set $\sigma = 0$ throughout our analysis and suppress the symbol σ everywhere. Thus, we find

$$\Phi_{00\mathbf{k}}(z) = -\frac{\pi^2 + k^2}{\pi\bar{C}} (\cos(\pi z) + 1). \tag{31}$$

The growth rate at this order is found to be

$$\sigma_0 = (\pi^2 + k^2) \left(\frac{Q_{00}}{Q_{00}(k)} - 1 \right), \tag{32}$$

where $Q_{00}(k)$ describes the neutral curve

$$Q_{00}(k) = \frac{(\pi^2 + k^2)^2}{k^2}. \tag{33}$$

The neutral curve (33) has a minimum of $Q_c = 4\pi^2$ at the critical wavenumber $k_c = \pi$. These results, along with the expressions for the temperature and velocity fields, correspond to those obtained for steady thermal convection in a passive porous medium (Lapwood 1948). The effects of dissolution enter the perturbative analysis at higher order.

3.2. Weakly nonlinear analysis

The perturbation expansion is then carried out under the usual prescription; at each step in the expansion, we obtain a system of linear, inhomogeneous ordinary differential equations (given explicitly in appendix B) of the form

$$\mathcal{L}_{00}\mathbf{v}_{mn} = \mathcal{I}_{mn}. \tag{34}$$

A nonsecular solution to (34) exists if and only if the inhomogeneities \mathcal{I}_{mn} are orthogonal to the solutions $\hat{\mathbf{v}}$ of the adjoint problem, that is,

$$\int_0^1 dz \hat{\mathbf{v}} \cdot \mathcal{I}_{mn} = 0. \tag{35}$$

In the present problem, the differential operator (with its boundary conditions) is not self-adjoint.

The analysis performed parallels that of Anderson and Worster (1995). We push the effect of variation in the permeability to higher order by assuming

$$\mathcal{K}_1 = \epsilon \bar{\mathcal{K}}_1 = \mathcal{O}(\epsilon). \quad (36)$$

In addition, we preserve spatial information by allowing the wave-vector \mathbf{k} to vary over all directions in its plane while keeping its magnitude $|\mathbf{k}| = k$ very close to the critical wavenumber k_c . We further add the approximation that the support of the wavenumber spectrum of the modes included in the analysis is confined to the narrow annulus around $k \approx k_c$ mentioned previously.

This last condition, which amounts to an assumption of compact support for $\tilde{f}_{\mathbf{k}}$, circumvents a difficulty arising in the derivation of the pattern equation for systems with continuous spectra, namely that, to our knowledge, no centre manifold theorem has been proved for extended systems with continuous spectra. The failure to extend this useful theorem may probably be blamed on the presence of irremovable resonances among stable modes that appear in the form of a factor $(\sigma(\mathbf{p}) + \sigma(\mathbf{q}) - s(\mathbf{k}))^{-1}$, where $\mathbf{k} = \mathbf{p} + \mathbf{q}$ is a triad of wavenumbers with associated linear growth rates σ , $s(\mathbf{k}) = -|\sigma(\mathbf{k})|$ is the (strictly negative) growth rate of a stable (damped) mode and $\sigma(\mathbf{k})$ is negative everywhere except within a narrow band of wavenumbers centred on k_c (Couillet and Spiegel 1988, Cessi *et al.* 1990). In all derivations of the Swift–Hohenberg equation of which we are aware, such singularities are avoided (sometimes implicitly), hence our assumption of compact support of the modal spectrum.

At $\mathcal{O}(\epsilon^1 \delta^0)$, the equations to be solved are

$$\mathcal{L}_{00\mathbf{k}} \tilde{\mathbf{v}}_{10\mathbf{k}} = \tilde{\mathbf{N}}_{10\mathbf{k}} - \mathcal{L}_{10\mathbf{k}} \tilde{\mathbf{v}}_{00\mathbf{k}}, \quad (37)$$

so that the $\mathcal{O}(\epsilon^0 \delta^0)$ solutions appear as inhomogeneous terms on the right-hand side of (37).

The solvability condition at this order gives

$$\mathcal{Q}_{10} \equiv 0. \quad (38)$$

This is a direct consequence of the assumption that $\mathcal{K}_1 = \epsilon \bar{\mathcal{K}}_1 = \mathcal{O}(\epsilon)$. The $\mathcal{O}(\epsilon^1 \delta^0)$ fields are found to be

$$\tilde{\phi}_{10,\mathbf{k}} = -\frac{\pi^2 + k^2}{\pi \bar{C}} [\cos(\pi z) + 1 + a(\mathbf{k}) (\cos(2\pi z) - 1)], \quad (39a)$$

$$\tilde{\theta}_{10,\mathbf{k}} = -\sin(\pi z) - b(\mathbf{k}) \sin(2\pi z), \quad (39b)$$

$$\tilde{w}_{10,\mathbf{k}} = (\pi^2 + k^2) (\sin(\pi z) + c(\mathbf{k}) \sin(2\pi z)), \quad (39c)$$

where

$$a(\mathbf{k}) = \frac{(4\pi^2 + k^2)^2}{(5\pi^2 + 2k^2)(\pi^2 + k^2)} \frac{F(\mathbf{k})}{6\pi^2}, \quad b(\mathbf{k}) = \frac{4\pi^2 + k^2}{5\pi^2 + 2k^2} \frac{F(\mathbf{k})}{3\pi^2}, \quad c(\mathbf{k}) = \frac{\pi^2 + k^2}{5\pi^2 + 2k^2} \frac{F(\mathbf{k})}{3\pi^2}, \quad (40a,b,c)$$

and

$$F(\mathbf{k}) = \frac{\pi}{2} \int_{\mathbf{k}=\mathbf{p}+\mathbf{q}} d\mathbf{p} d\mathbf{q} (\pi^2 + p^2) \left(\frac{\mathbf{p} \cdot \mathbf{q}}{p^2} - 1 \right). \quad (40d)$$

At $O(\epsilon^2\delta^{-1})$ we find

$$\partial_T \tilde{\phi}_{00\mathbf{k}} = \partial_z \tilde{\phi}_{2,-1\mathbf{k}}, \quad (41)$$

so that

$$\tilde{\phi}_{2,-1\mathbf{k}} = -\frac{\pi^2 + k^2}{\pi \bar{C}} \left(\frac{\sin(\pi z)}{\pi} + (z - 1) \right) \partial_T \tilde{f}_{\mathbf{k}}. \quad (42)$$

Finally, at $O(\epsilon^2\delta^0)$ we have

$$\mathcal{L}_{00\mathbf{k}} \tilde{\mathbf{v}}_{20\mathbf{k}} = \tilde{\mathbf{N}}_{20\mathbf{k}} - \mathcal{L}_{01\mathbf{k}} \tilde{\mathbf{v}}_{2,-1\mathbf{k}} - \mathcal{L}_{10\mathbf{k}} \tilde{\mathbf{v}}_{10\mathbf{k}} - \mathcal{L}_{20\mathbf{k}} \tilde{\mathbf{v}}_{00\mathbf{k}} - \mathcal{T}_{0,-1\mathbf{k}} \partial_T \tilde{\mathbf{v}}_{01\mathbf{k}} - \mathcal{T}_{00\mathbf{k}} \tilde{\mathbf{v}}_{00\mathbf{k}}. \quad (43)$$

As a consequence of $Q_{10} = 0$, the term proportional to $\mathcal{L}_{10\mathbf{k}}$ makes no contribution. We show in appendix C that the solvability condition for (43) gives the pattern equation

$$\lambda_{\mathbf{k}} \partial_T \tilde{f}_{\mathbf{k}} = 2 \frac{Q_{20} k^2}{\pi^2 + k^2} \tilde{f}_{\mathbf{k}} + M_{\mathbf{k}} \{ \tilde{f}^2 \} - N_{\mathbf{k}} \{ \tilde{f}^3 \}, \quad (44)$$

for the planform $\tilde{f}_{\mathbf{k}}$, where

$$M_{\mathbf{k}} \{ \tilde{f}^2 \} \equiv \int_{\mathbf{k}=\mathbf{p}+\mathbf{q}} \mathbf{d}\mathbf{p} \mathbf{d}\mathbf{q} \mathcal{M}_{\mathbf{pq}}^{\mathbf{k}} \tilde{f}_{\mathbf{p}} \tilde{f}_{\mathbf{q}}, \quad (45a)$$

$$N_{\mathbf{k}} \{ \tilde{f}^3 \} \equiv \frac{1}{3} \int_{\mathbf{k}=\mathbf{l}+\mathbf{m}+\mathbf{n}} \mathbf{d}\mathbf{l} \mathbf{d}\mathbf{m} \mathbf{d}\mathbf{n} \left(\mathcal{N}_{\mathbf{lmn}}^{\mathbf{k}} + \mathcal{N}_{\mathbf{nml}}^{\mathbf{k}} + \mathcal{N}_{\mathbf{mln}}^{\mathbf{k}} \right) \tilde{f}_{\mathbf{l}} \tilde{f}_{\mathbf{m}} \tilde{f}_{\mathbf{n}}, \quad (45b)$$

where

$$\mathcal{M}_{\mathbf{pq}}^{\mathbf{k}} = \mathcal{M}_{\mathbf{qp}}^{\mathbf{k}} = \frac{2\pi \bar{\mathcal{K}}_1}{\bar{C} + \bar{S}} \frac{(\pi^2 + p^2)(\pi^2 + q^2)}{(\pi^2 + k^2)} \left\{ \frac{\mathbf{p} \cdot \mathbf{q}}{2} \left(\frac{1}{p^2} + \frac{1}{q^2} \right) + \frac{\pi^2 + k^2}{\pi^2} \right\} \quad (46)$$

and the kernel $\mathcal{N}_{\mathbf{lmn}}^{\mathbf{k}}$ is given in appendix C.

The coefficient $\lambda_{\mathbf{k}}$ in front of the time derivative in the pattern equation (44) is given by

$$\lambda_{\mathbf{k}} = \Omega - \frac{\pi^2 + k^2}{\pi^2} \frac{\bar{S}}{\Omega \bar{C}^2}. \quad (47)$$

Thus, $\lambda_{\mathbf{k}}$ may be negative or even vanish. As Anderson and Worster (1995) have noted, this indicates the presence of a Hopf bifurcation. In this work, we do not consider that regime of parameter values and consider the direct mode only. A derivation of the full pattern equation in the presence of a Hopf bifurcation may be carried out in the manner we have described for the stationary case. In the meantime, close to marginality ($|\mathbf{k}| \approx k_c$) we obtain the result of Anderson and Worster (1995),

$$\lambda_{\mathbf{k}} \approx \lambda_c = \Omega - \frac{2\bar{S}}{\Omega \bar{C}^2}. \quad (48)$$

For definiteness, we shall assume that λ_c is positive and finite: setting λ_c negative is equivalent to reversing the sign of the planform f , which in turn is equivalent to reversing the sign of the coefficient $\mathcal{M}_{\mathbf{k}}$. We discuss the effect of such a sign-reversal below.

Close to marginality, the coefficient of the linear term on the right-hand side of (44) can be expressed as

$$\frac{Q_{20}k^2}{\pi^2 + k^2} \approx \frac{\pi^2 + k^2}{\epsilon^2} \left(\frac{Q}{Q_{00}(k)} - 1 \right) = \frac{\sigma_0}{\epsilon^2}. \quad (49)$$

Note that close to marginality $Q \approx Q_{00}(\mathbf{k}) \approx Q_c$ so that

$$\epsilon^2 = \frac{Q - Q_c}{Q_{20}}, \quad (50)$$

which defines ϵ precisely.

Expanding about the critical wavenumber $k_c = \pi$ we find that

$$\frac{\sigma_0}{\epsilon^2} \approx \frac{2\pi^2}{\epsilon^2} \left[\frac{Q - Q_c}{Q_c} - \frac{1}{4} \left(\frac{k^2}{\pi^2} - 1 \right)^2 \right] = \rho - \ell_{\mathbf{k}}, \quad (51a)$$

with

$$\rho = \frac{2\pi^2}{\epsilon^2} \frac{Q - Q_c}{Q_c} = \mathcal{O}(1), \quad \ell_{\mathbf{k}} = \frac{(k^2 - k_c^2)^2}{2\pi^2 \epsilon^2} = \mathcal{O}(1). \quad (51b)$$

Thus we see that ρ measures the departure of the Rayleigh number from its critical value and $\ell_{\mathbf{k}}$ is proportional to the Fourier transform of the familiar Swift–Hohenberg linear operator $(\nabla^2 + k_c^2)^2$.

Finally, we find that, under suitable rescaling of both space and time, the pattern equation for the planform $f = f(x, y)$ becomes, in real space,

$$\partial_T f = \rho f - (\nabla_H^2 + k_c^2)^2 f + M\{f^2\} - N\{f^3\}. \quad (52)$$

If the kernels $\mathcal{M}_{\mathbf{k}\mathbf{p}\mathbf{q}}$ and $\mathcal{N}_{\mathbf{k}\mathbf{l}\mathbf{m}\mathbf{n}}$ are replaced with coefficients μ and ν , respectively, (52) takes the real space form of a Swift–Hohenberg equation with a quadratic term term (Swift and Hohenberg 1977, Bestehorn and Haken 1983):

$$\partial_T f = \rho f - (\nabla_H^2 + k_c^2)^2 f + \mu f^2 - \nu f^3. \quad (53)$$

The primary motivation for deriving a general pattern equation for a planform $\tilde{f}_{\mathbf{k}}$ (or, in real space, $f(x, y, T)$) was to avoid making any *a priori* assumptions about the pattern. Rather, one can prescribe some arbitrary initial state (e.g. a random one) and, with the aid of a small computer, investigate its evolution. For pattern equations of the Swift–Hohenberg type, one typically sees a number of patterns competing with one another until the planform settles into a fixed pattern and evolves no further (see, for instance, Cross and Hohenberg (1993) and references therein). Such equations exhibit many quasi-stationary patterns, including, but not limited to, the hexagons, rolls, and mixed modes studied by Amberg and Homsy (1993) and Anderson and Worster (1995).

The principal difference between the derived pattern equation (52) and the generic Swift–Hohenberg equation (53) is the dependence of the coefficients $\mathcal{M}_{\mathbf{k}}$ and $\mathcal{N}_{\mathbf{k}}$ upon the spatial distribution of the planform. In particular, we note that $\bar{\mathcal{K}}_1$, \bar{C} and \bar{S} are all positive (by construction), but $\mathcal{M}_{\mathbf{p}\mathbf{q}}^{\mathbf{k}}$ can take either sign, depending on the members of

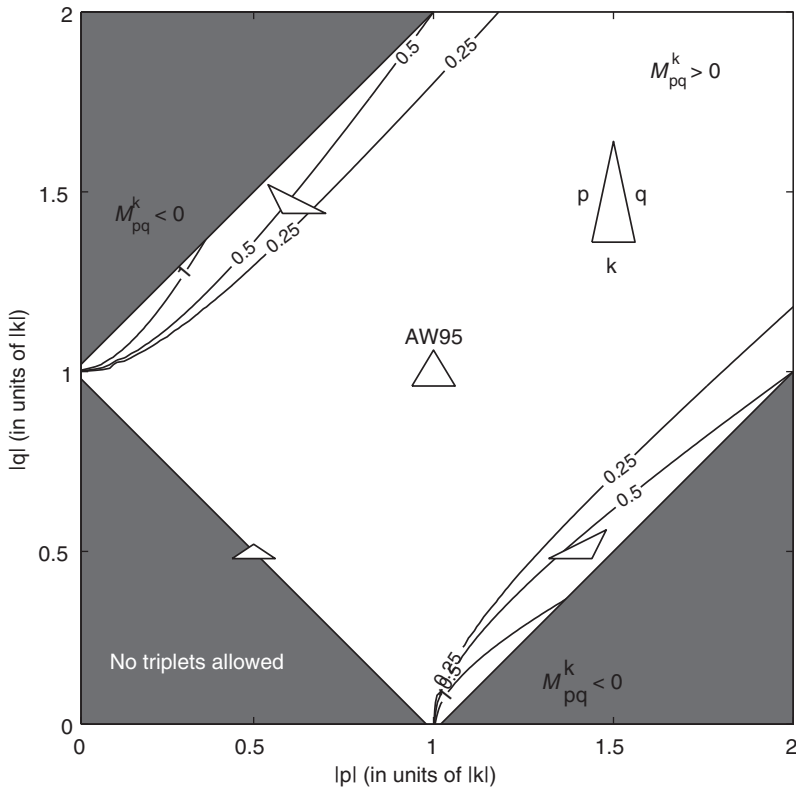


Figure 3. The sign of M_{pq}^k as a function of $|p|$ and $|q|$. Grey regions represent triplets that cannot satisfy the constraint $\mathbf{k} = \mathbf{p} + \mathbf{q}$. The value of $|k|$ (in units of $k_c = \pi$) where M_{pq}^k changes sign is indicated by the contours on either side of the main diagonal. The triplet labelled AW95 denotes the case of $|k| = |p| = |q| = \pi$ considered by Anderson and Worster (1995).

the triplet $\mathbf{k} = \mathbf{p} + \mathbf{q}$. Thus,

$$M_{pq}^k \geq 0 \quad \text{when} \quad k^2 \geq \frac{\pi^2(p^2 - q^2)^2}{\pi^2(p^2 + q^2) + 4p^2q^2}, \quad (54)$$

and is negative otherwise. By holding $|k|$ fixed, the transition from positive to negative M_{pq}^k can be depicted on the pq -plane (figure 3). Because the members of the triplet must satisfy $\mathbf{k} = \mathbf{p} + \mathbf{q}$, no one member can be larger than the sum of the other two, as represented by the grey regions in figure 3. Along the diagonal $|p| = |q|$, (54) is automatically satisfied for all $|k|$, and so M_{pq}^k is always non-negative for these triplets. This subset includes the triplet $|k| = |p| = |q| = \pi$ considered by Anderson and Worster (1995; denoted by AW95 in figure 3). For asymmetrical triplets, however, M_{pq}^k can take on negative values; the value of $|k|$ (in units of $k_c = \pi$) where this occurs is indicated by the contours on either side of the main diagonal. The overall sign of $M_{\mathbf{k}}$ then depends on the relative population of symmetrical and asymmetrical triplets.

Thus the sign of both λ and M can change depending on the values of the experimental parameters *and* the spatial distribution of the planform f . Since changing the sign of either λ and M is equivalent to changing the sign of f , this means that both

Table 1. Direction of flow at centre of hexagons.
The first two rows reproduce the results of
Anderson and Worster (1995).

$M > 0$	$\lambda > 0$	upwelling
$M > 0$	$\lambda < 0$	downwelling
$M < 0$	$\lambda > 0$	downwelling
$M < 0$	$\lambda < 0$	upwelling

up and down flow states are possible (table 1). These results stand in contrast to those of Anderson and Worster (1995), who found that the direction of flow at the centre of hexagons was determined by the sign of λ alone. We note that, to date, the only experimental observations of hexagons are those of Tait and Jaupart (1992), who observed upflow at the edges and downflow in the centres of hexagons.

Finally, we observe that the linear operator $(\nabla_H^2 + k_c^2)^2$ establishes k_c as the dominant wavenumber at $\rho = 0$. In these conditions it is possible to evaluate the integrals $M_{\mathbf{k}}\{\tilde{f}^2\}$ and $N_{\mathbf{k}}\{\tilde{f}^3\}$ explicitly. That is, we assume that $\tilde{f}_p = F(\alpha_p)\pi^{-1}\delta(|\mathbf{p}| - k_c)$, where α_p is the angle \mathbf{p} makes with $\mathbf{k} = k\hat{\mathbf{x}}$. In appendix C we show that, under the assumption of compact support for $\tilde{f}_{\mathbf{k}}$,

$$\mathcal{M}_{\mathbf{k}}\{\tilde{f}^2\} = 6\pi^2 \frac{\bar{\mathcal{K}}_1}{\bar{C} + \bar{S}} F\left(\frac{\pi}{3}\right) F\left(-\frac{\pi}{3}\right), \quad (55a)$$

$$\mathcal{N}_{\mathbf{k}}\{\tilde{f}^3\} = \frac{8\pi^6}{3} \int_0^{2\pi} d\alpha \left\{ \frac{3\mathcal{K}_2}{2(\bar{C} + \bar{S})^2} A(\alpha) + B(\alpha) \right\} F(0)F(\alpha)F(\alpha - \pi). \quad (55b)$$

The geometrical functions $A(\alpha)$ and $B(\alpha)$ have the form

$$A(\alpha) = 11 + 7 \cos \alpha, \quad B(\alpha) = (1 + \cos \alpha)^2 \frac{3 - \cos \alpha}{9 - 4 \cos \alpha}. \quad (56)$$

When all wavevectors are of the same length, only certain tessellations will be selected by the delta functions present in the integrands. In particular, when \mathbf{k} , \mathbf{p} and \mathbf{q} are all of the same length ($k_c = \pi$), the triplet must form an equilateral triangle. Consequently, we may associate the quadratic term appearing in (52) with a planform made up of three rolls superposed at 120° , as depicted in figure 4(a).

In the case of the cubic term, the quadruple $\{\mathbf{k}, \mathbf{l}, \mathbf{m}, \mathbf{n}\}$ must satisfy $\mathbf{k} = \mathbf{l} + \mathbf{m} + \mathbf{n}$, so that $\{\mathbf{k}, \mathbf{l}, \mathbf{m}, \mathbf{n}\}$ form an equilateral parallelogram (figure 4(b)), with arbitrary angle α between \mathbf{k} and \mathbf{l} (say). Hence, both rolls ($\alpha \equiv 0$) and hexagons ($\alpha \in \{0, \pi/3, 2\pi/3\}$) are special cases of the general system. It is evident, then, that the simplified pattern equation (53) preserves many of the qualitative features of the full problem.

4. Dynamics of interacting chimney-like solutions

The Swift–Hohenberg equation (53) should be considered as a highly simplified model capable of reproducing some of the qualitative features of the more complicated full pattern equation (52). This strategy has provided a great deal of insight in other

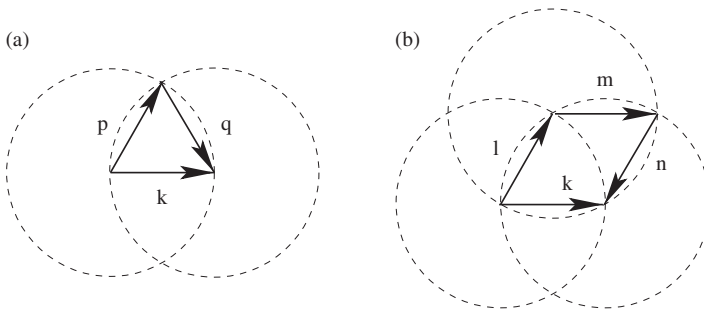


Figure 4. (a) Allowed tessellations satisfying the condition $\mathbf{k} = \mathbf{p} + \mathbf{q}$. (b) Allowed tessellations satisfying the condition $\mathbf{k} = \mathbf{l} + \mathbf{m} + \mathbf{n}$. The quadruple $\{\mathbf{k}, \mathbf{l}, \mathbf{m}, \mathbf{n}\}$ forms an equilateral parallelogram with interior angle α . If all four wavevectors lie along the same axis, this corresponds to the case of three interacting one-dimensional rolls.

convective pattern formation problems (see, e.g. Cross and Hohenberg 1993), and it is in this spirit that we examine, in this section, the transient evolution of patterns in mushy layers and, in particular, the dynamics of widely separated chimney-like solutions of (53).

For motion confined to the xz -plane, the pattern equation (52) reduces to

$$\partial_T f = \rho f - (\partial_x^2 + k_c^2)^2 f - \nu f^3, \tag{57}$$

since μ is necessarily zero as a consequence of the fact that the constraint $\mathbf{k} = \mathbf{p} + \mathbf{q}$ appearing in (C.5a), the expression for $\mathcal{M}\{f^2\}$, cannot be satisfied in one horizontal spatial dimension. Let us consider the dynamics of “chimney-like” solutions to (57). True chimneys are regions of zero solid fraction and the flow within these regions is no longer governed by Darcy’s law. Here, we will examine localized minima of the solid fraction, or, equivalently, extrema of the planform $f(\mathbf{x}, T)$, which we shall refer to as “spikes”. These localized solutions can be considered to be nascent chimneys that still satisfy the weakly nonlinear constraint. Far from the spike itself, the nonlinear terms in the pattern equation can be neglected in the first approximation, so that the asymptotic behaviour of the planform is given by $e^{-m|x|}$ as $|x| \rightarrow \infty$, where $m = \sqrt{\rho^{1/2} - k_c^2}$. For $\rho \geq k_c^4$ localized solutions exist (Burke and Knobloch 2006). As long as the spikes remain separated by a distance L that is large compared to the spike radius then $\gamma = e^{-mL}$ plays the role of a small parameter, and the dynamics of widely separated spikes can be investigated (see Elphick *et al.* 1990, Balmforth 1995, and references therein).

Let us assume that the pattern equation possesses isolated spike solutions of the form $f = h(x)$

$$\left(\rho - (\partial_x^2 + k_c^2)^2\right)h - \nu h^3 = 0. \tag{58}$$

The general solution can be approximated as a linear superposition of N widely spaced spikes, plus some small remainder, γr , which is a function of the slow timescale $\tau = \gamma t$ and the set of spike positions $\{x_i\}$. Thus

$$f = \sum_{n=1}^N h_n + \gamma r(\{x_i\}, \tau), \quad h_n = h(x - x_n(\tau)). \tag{59}$$

On substituting (59) into the one-dimensional pattern equation (57), we obtain

$$0 = \gamma \sum_{n=1}^N \frac{dh_n}{dx} \frac{dx_n}{d\tau} - \gamma^2 \frac{dr}{d\tau} + \left(\rho - (\partial_x^2 + k_c^2)^2 \right) \left(\sum_{n=1}^N h_n + \gamma r \right) - v \left(\sum_{n=1}^N h_n + \gamma r \right)^3. \quad (60)$$

Making use of (58) and keeping only the lowest order terms, we find that

$$\mathcal{H}r = \sum_{n=1}^N \frac{dh_n}{dx} \frac{dx_n}{d\tau} - \gamma^{-1} v \left[\left(\sum_{n=1}^N h_n \right)^3 - \sum_{n=1}^N h_n^3 \right], \quad (61a)$$

where the operator \mathcal{H} is

$$\mathcal{H} = - \left(\rho - (\partial_x^2 + k_c^2)^2 \right) + 3v \left(\sum_{n=1}^N h_n \right)^2. \quad (61b)$$

The nonlinear expression on the right-hand side of (61a) is, despite appearances, $\mathcal{O}(1)$, as can be seen by writing the term in brackets as

$$\sum_{n=1}^N h_n \left(h_n + \sum_{m \neq n} h_m \right)^2 - \sum_{n=1}^N h_n^3 = \sum_{n=1}^N h_n \left[2h_n \sum_{m \neq n} h_m + \left(\sum_{m \neq n} h_m \right)^2 \right]. \quad (62)$$

From the assumption that the spikes are widely spaced it follows that $h_{n \pm 1} = \mathcal{O}(\gamma)$, $h_{n \pm 2} = \mathcal{O}(\gamma^2)$, and so on. Thus, (61a) becomes,

$$\mathcal{H}r = \sum_{n=1}^N \frac{dh_n}{dx} \frac{dx_n}{d\tau} - 2\gamma^{-1} v \sum_{n=1}^N h_n^2 (h_{n-1} + h_{n+1}) + \mathcal{O}(\gamma), \quad (63a)$$

with

$$\mathcal{H} = - \left(\rho - (\partial_x^2 + k_c^2)^2 \right) + 3v \sum_{n=1}^N h_n^2. \quad (63b)$$

As discussed in Elphick *et al.* (1990), the operator \mathcal{H} is reminiscent of the Hamiltonian operator appearing in the Schrödinger equation for an electron moving in a lattice potential. As in the tight binding approximation of solid state physics, we may expect that r , which corresponds to the electron wave function, will be concentrated near the lattice points, that is, the spikes. For widely separated spikes, therefore, the eigenfunctions of \mathcal{H} can be approximated by the eigenfunctions of

$$\mathcal{H}_n = - \left(\rho - (\partial_x^2 + k_c^2)^2 \right) + 3v h_n^2. \quad (64)$$

As can be seen by differentiating (58) with respect to x , the eigenfunction of \mathcal{H}_n with eigenvalue zero is $\partial_x h_n$. Using the self-adjointness of the operator \mathcal{H} , we see that $\partial_x h_n$ is the solution to the adjoint equation. Thus, the solvability condition for (63a) implies

$$\langle \partial_x h_n | \partial_x h_n \rangle \partial_\tau x_n - 2v\gamma^{-1} \langle \partial_x h_n | h_n^2 (h_{n-1} + h_{n+1}) \rangle = \mathcal{O}(\gamma), \quad (65)$$

where $\langle f | g \rangle$ is the inner product of functions f and g .

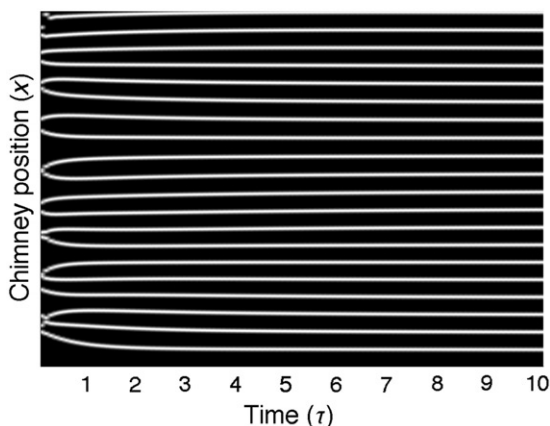


Figure 5. Evolution of $N=20$ initially randomly distributed spikes (shown in white on a black background) in a periodic domain. Time, increasing to the right, has been rescaled to absorb the coefficient A .

The solvability condition (65) represents a dynamical equation for x_n , the position of the n th spike, in terms of the positions of its nearest neighbours $x_{n\pm 1}$. As we are integrating over all x , the detailed structure of h is not important. Since x_n is assumed to be far from both $x_{n\pm 1}$, we can take

$$h_{n+1} \approx h_0 e^{my} e^{-m(x_{n+1}-x_n)}, \quad h_{n-1} \approx h_0 e^{-my} e^{-m(x_n-x_{n-1})} \quad (66a,b)$$

where $y = x - x_n$ and h_0 is a constant. The dynamical equation for $x_n(\tau)$ then becomes

$$\frac{dx_n}{d\tau} = A_+ e^{-m(x_{n+1}-x_n)} + A_- e^{-m(x_n-x_{n-1})}, \quad (67a)$$

where

$$A_{\pm} = 2v\gamma^{-1}h_0 \int dy (\partial_y h(y))h(y)e^{\pm my} / \int dy (\partial_y h(y))^2. \quad (67b)$$

Symmetry of $h(y)$ under $y \rightarrow -y$ implies that $A_+ = -A_-$. Therefore, the displacement $\chi_n = x_n - nL$ of the n th spike from its lattice point is given by

$$\frac{d\chi_n}{d\tau} = e^{-m(\chi_{n+1}-\chi_n)} - e^{-m(\chi_n-\chi_{n-1})}, \quad (68)$$

where the constants A_{\pm} have been absorbed into τ , and, with them, all information about the detailed internal structure of the spike solution.

The dynamical equation (68) has the form of a non-inertial damped motion of a particle interacting with its nearest neighbours. Figure 5 depicts the evolution of $N=20$ (initially) randomly distributed spikes in a periodic domain, with $m=1$. As can be seen, the spikes attain the uniform spacing L on the decay timescale $\tau = A\gamma t = 1$. Figure 6 shows the effect of introducing or removing a spike on the evolution of $N=10$ spikes in a periodic domain. The spikes are evolved for $\tau=5$ time units and establish a uniform lattice, after which a spike is either added (left) or removed (right) by hand. Subsequently, the spikes establish a new lattice, with a correspondingly larger or smaller lattice spacing.

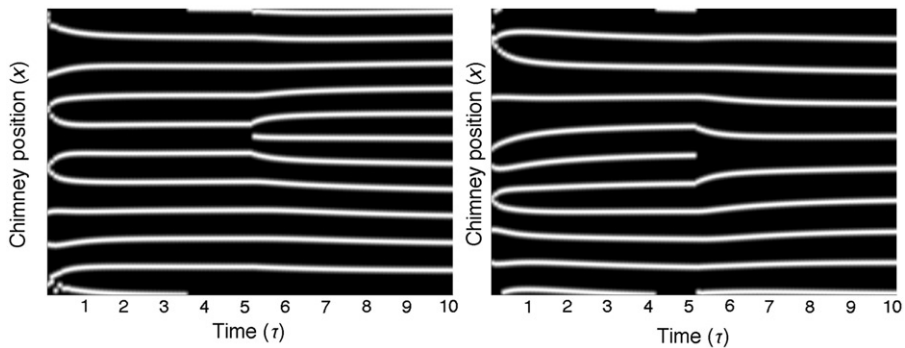


Figure 6. Effect of defects on the evolution of $N = 10$ spikes in a periodic domain. In both cases, the spikes evolve for 5 time units, establishing a regular arrangement. At $\tau = 5$, a spike is introduced (*left*) or removed (*right*), after which point the spikes rearrange into a regular lattice of different spacing.

It is worth pointing out that (68) does not give a prediction of the spacing between spikes; in this regard, the theory we have outlined shares the inability of weakly nonlinear convective theories in determining the horizontal scale of convective cells. In principle, one could develop an energy stability theory for the pattern equation (52) and hence obtain a prediction for the separation of weak chimneys in one or two dimensions. Such a calculation is beyond the scope of this initial study, however, and remains an interesting topic for further research.

5. Discussion

As we have noted, the pattern equation derived in section 3 has the form of a Swift–Hohenberg equation with an additional quadratic term. The Swift–Hohenberg equation arises in a wide variety of physical, chemical and biological contexts and has a substantial literature associated with it (see Cross and Hohenberg (1993) and references therein for a comprehensive review of this topic).

The quadratic term appearing in the pattern equation (52) destroys the symmetry between up and down of the Boussinesq approximation for which hexagonal planforms with either up-flow or down-flow at the centre have equal dissipation rates. This is perhaps not surprising when one notes that, unlike other planforms, which exchange up and down by translation of a half cell, hexagonal convection cells are manifestly asymmetric.

This quadratic term is associated, via the constraints $\mathbf{k} = \mathbf{p} + \mathbf{q}$ and $k \approx k_c$, to planforms made up of three rolls superposed at nearly 120° to one another. If all three rolls have the same equal amplitude and the angle is 120° , the unit cell is a hexagon. Thus, we recover the result of Amberg and Homsy (1993) that the transition to three-dimensional hexagons is transcritical. The sign of the quadratic term is set by the relative populations of symmetric and asymmetric triplets, and it is this term, in conjunction with the experimental parameters \bar{C} and \bar{S} that determines whether there is up-flow or down-flow at the centres of the hexagons.

We also note that the expression for the quadratic term $M\{f^2\}$ is proportional to \bar{K}_1 . Thus, symmetry breaking between up-flow and down-flow at the centre of hexagons is rooted in the non-Boussinesq effect of permeability variation with solid fraction. As \bar{K}_1 is

strictly positive on physical grounds, the overall sign of the quadratic term is determined by the spatial distribution of the planform f itself, at least in this pared down model.

As we have discussed, the principal advantage of, and motivation for, the pattern equation derived here is that it enables one to investigate the spatial structure of weakly nonlinear convection in a mushy layer without preselecting the pattern. That the equation thus derived has the form of a Swift–Hohenberg equation demonstrates that convection in a mushy layer bears many similarities with other convection problems, although with its own distinctive character arising from the interaction of dissolution, solidification and permeability variation.

In addition to the insight gained into spatial structure, these pattern equations also allow us to make a beginning of the study of transient evolution of patterns of convection in a mushy layer. Such transient behaviour has been observed in a number of experiments (Tait *et al.* 1992, Peppin *et al.* 2008), but has not been examined theoretically. The approximations we invoke in our derivation, such as weak nonlinearity, constant mush depth and constant speed of solidification, mean that the pattern equation we obtain is not appropriate for a quantitative description of such transient behaviour. However, some interesting qualitative features can be described using a simplified one-dimensional approximation of the full pattern equation. To that end, we examined the interaction of widely separated “spikes” – extrema of the planform corresponding to nascent chimney-like structures – and derived an equation describing their dynamics. Numerical simulations of the spikes quickly achieve uniform spacing and can robustly adapt to an increase or decrease in the spike number.

Acknowledgements

The bulk of this work was carried out at the Woods Hole Oceanographic Institute geophysical fluid dynamics summer programs in 2006 and 2007, which have received support from NSF grant number OCE 03-25296 and ONR grant number N00014-07-1-0776. The authors thank the directors of these programs, in particular Neil Balmforth and John Wettlaufer. We also thank Andrew Fowler and Yiping Ma for useful discussions.

References

- Amberg, G. and Homsy, G., Nonlinear analysis of buoyant convection in binary solidification with applications to channel formation. *J. Fluid Mech.* 1993, **252**, 79–98.
- Anderson, D. and Worster, M.G., Weakly nonlinear analysis of convection in mushy layers during the solidification of binary alloys. *J. Fluid Mech.* 1995, **302**, 307–331.
- Anderson, D. and Worster, M.G., A new oscillatory instability in a mushy layer during the solidification of binary alloys. *J. Fluid Mech.* 1996, **307**, 245–267.
- Balmforth, N., Solitary waves and homoclinic orbits. *Ann. Rev. Fluid Mech.* 1995, **27**, 335–375.
- Bestehorn, M. and Haken, H., A calculation of transient solutions describing roll and hexagon formation in the convection instability. *Phys. Lett. A* 1983, **99**, 265–267.
- Burke, J. and Knobloch, E., Localized states in the generalized Swift–Hohenberg equation. *Phys. Rev. E* 2006, **73**, 056211-1-15.
- Cessi, P., Spiegel, E. and Young, W., Small-scale excitations in large systems. In *Nonlinear Evolution of Spatiotemporal Structures in Dissipative, Continuous Systems*, edited by F. Busse and K. Kramer, Vol. 255 of *NATO ASI Series*, pp. 231–236, 1990. (Plenum Press, New York).

- Chen, F., Lu, J. and Yang, T., Convective instability in ammonium chloride solution directionally solidified from below. *J. Fluid Mech.* 1994, **276**, 163–187.
- Chung, C. and Chen, F., Onset of plume convection in mushy layers. *J. Fluid Mech.* 2000, **408**, 53–82.
- Coulet, P. and Spiegel, E., Evolution equations for extended systems. In *Energy Stability and Convection*, edited by G. Galdi and B. Straughan, Pitman Research Notes in Math (Vol. 168), p. 22, 1988. (Longman Science and Technology: New York).
- Cross, M., Derivation of the amplitude equation at the Rayleigh–Bernard instability. *Phys. Fluids* 1980, **23**, 1727–1731.
- Cross, M. and Hohenberg, P., Pattern formation outside of equilibrium. *Rev. Mod. Phys.* 1993, **65**, 851–1112.
- Davis, S.H., *Theory of Solidification*, 2001. (Cambridge: Cambridge University Press).
- Elphick, C., Meron, E. and Spiegel, E.A., Patterns of propagating pulses. *SIAM J. Appl. Math.* 1990, **50**, 490–503.
- Fowler, A., The formation of freckles in binary alloys. *IMA J. Appl. Maths* 1985, **35**, 159–174.
- Guba, P. and Worster, M.G., Nonlinear oscillatory convection in mushy layers. *J. Fluid Mech.* 2006, **553**, 419–443.
- Haken, H., *Advanced Synergetics*, 1983. (Berlin: Springer).
- Huppert, H.E., The fluid mechanics of solidification. *J. Fluid Mech.* 1990, **212**, 209–240.
- Lapwood, E.R., Convection of a fluid in a porous medium. *Proc. Camb. Phil. Soc* 1948, 508–521.
- Ma, Y., The derivation and application of convective pattern equations. In *Proceedings of the 2009 Woods Hole Oceanographic Institution Geophysical Fluid Dynamics Summer School*, pp. 308–329, 2009. (WHOI: Woods Hole, MA).
- Manneville, P., *Dissipative Structures and Weak Turbulence*, 1990. (Berlin, Heidelberg: Springer).
- Peppin, S., Huppert, H. and Worster, M.G., Steady-state solidification of aqueous ammonium chloride. *J. Fluid Mech.* 2008, **599**, 465–476.
- Riahi, D., On nonlinear convection in mushy layers Part 1. Oscillatory modes of convection. *J. Fluid Mech.* 2002, **467**, 331–359.
- Riahi, D., On nonlinear convection in mushy layers. Part 2. Mixed oscillatory and stationary modes of convection. *J. Fluid Mech.* 2004, **517**, 71–101.
- Roper, S.M., Davis, S.H. and Voorhees, P.W., An analysis of convection in a mushy layer with a deformable permeable interface. *J. Fluid Mech.* 2008, **596**, 333–352.
- Swift, J.B. and Hohenberg, P.C., Hydrodynamic uctuations at the convective instability. *Phys. Rev. A* 1977, **15**, 319.
- Tait, S., Jahrling, K. and Jaupart, C., The planform of compositional convection and chimney formation in a mushy layer. *Nature* 1992, **359**, 406–408.
- Tait, S. and Jaupart, C., Compositional convection in a reactive crystalline mush and melt differentiation. *J. Geophys. Res.* 1992, **97**, 6735–6756.
- Worster, M., Instabilities of the liquid and mushy regions during solidification of alloys. *J. Fluid Mech.* 1992, **237**, 649–669.
- Worster, M., Convection in mushy layers. *Ann. Rev. Fluid Mech.* 1997, **29**, 91–122.
- Worster, M.G., Solidification in fluids. In *Perspectives in Fluid Dynamics*, edited by G.K. Batchelor, H.K. Moffatt and M.G. Worster, pp. 393–446, 2000. (Cambridge University Press: Cambridge).
- Worster, M.G., Summer school on ice. In *Proceedings of the 2006 Woods Hole Oceanographic Institution Geophysical Fluid Dynamics Summer School*, edited by N. Balmforth and J. Wettlaufer, 2006. (WHOI: Woods Hole, MA).

Appendix A: Expressions for the linear operators \mathcal{L} and \mathcal{T} and nonlinearity \mathcal{N}

The linear operator \mathcal{L} acting upon the vector $\mathbf{v} = (\phi, \theta, u, v, w)$ and appearing in equation (22) is given by

$$\mathcal{L} = \begin{bmatrix} -\bar{S}\partial_z & \Omega(\nabla^2 + \delta\partial_z) & 0 & 0 & -\partial_z\theta_B \\ \left\{ \begin{array}{c} -\delta\bar{S}/\bar{C}(\theta_B\partial_z) \\ +\partial_z\theta_B \end{array} \right\} & \left\{ \begin{array}{c} \Omega[-\delta\bar{S}/\bar{C}(\phi_B\partial_z + \partial_z\phi_B)] \\ +\nabla^2 + \Omega\delta\partial_z \end{array} \right\} & 0 & 0 & -\Omega\partial_z\theta_B \\ 0 & -Q\partial_x\partial_z & \mathcal{G} + \mathcal{H} & 0 & -\partial_z\mathcal{K}(\phi_B)\partial_x \\ 0 & -Q\partial_y\partial_z & 0 & \mathcal{G} + \mathcal{H} & -\partial_z\mathcal{K}(\phi_B)\partial_y \\ 0 & Q\nabla_H^2 & 0 & 0 & \mathcal{G} \end{bmatrix}, \quad (\text{A.1})$$

where the operators \mathcal{G} and \mathcal{H} are given by

$$\mathcal{G} = \mathcal{K}(\phi_B)\nabla^2 + \partial_z\mathcal{K}(\phi_B)\partial_z, \quad \mathcal{H} = \partial_z^2\mathcal{K}(\phi_B) + \partial_z\mathcal{K}(\phi_B)\partial_z. \quad (\text{A.2a,b})$$

The linear operator \mathcal{T} appearing in equation (22) is given by

$$\mathcal{T} = \begin{bmatrix} \bar{S}/\delta & -\Omega & 0 & 0 & 0 \\ \bar{S}/\bar{C}\theta_B & -\Omega(\Omega - \bar{S}/\bar{C}\phi_B) & 0 & 0 & 0 \\ 0 & 0 & 0 & 0 & 0 \\ 0 & 0 & 0 & 0 & 0 \\ 0 & 0 & 0 & 0 & 0 \end{bmatrix}. \quad (\text{A.3a})$$

Finally, the nonlinearity \mathbf{N} appearing in equation (22) is given by

$$\mathbf{N} = \begin{bmatrix} \mathbf{u} \cdot \nabla\theta \\ \Omega\mathbf{u} \cdot \nabla\theta - \bar{S}/\bar{C}(\epsilon^2\partial_T - \delta\partial_z)(\phi\theta) \\ \partial_x(\mathbf{u} \cdot \nabla\hat{\mathcal{K}}) - \nabla^2(u\hat{\mathcal{K}}) \\ \partial_y(\mathbf{u} \cdot \nabla\hat{\mathcal{K}}) - \nabla^2(v\hat{\mathcal{K}}) \\ \partial_z(\mathbf{u} \cdot \nabla\hat{\mathcal{K}}) - \nabla^2(w\hat{\mathcal{K}}) \end{bmatrix}. \quad (\text{A.3b})$$

Note that $\epsilon\hat{\mathcal{K}} = \mathcal{K}(\phi_B + \epsilon\phi/\Omega) - \mathcal{K}(\phi_B)$ is of order ϵ , as can be seen from a Taylor expansion in powers of $\epsilon\phi/\Omega$,

$$\mathcal{K}(\phi_B + \epsilon\phi/\Omega) - \mathcal{K}(\phi_B) = \frac{\epsilon\phi}{\Omega}\dot{\mathcal{K}}(\phi_B) + \frac{1}{2}\left(\frac{\epsilon\phi}{\Omega}\right)^2\ddot{\mathcal{K}}(\phi_B) + \dots, \quad (\text{A.4})$$

where a dot represents differentiation with respect the the function's argument.

Appendix B: Finite-amplitude expansion of \mathcal{L} , \mathcal{T} , and \mathbf{N}

As a consequence of (27a,b), which expresses \tilde{u} and \tilde{v} in terms of \tilde{w} , the number of dynamical quantities reduces to three, that is $\tilde{\mathbf{v}} = (\tilde{\phi}, \tilde{\theta}, \tilde{w})$. Hence, the operators $\mathcal{L}_{m\mathbf{k}}$ and $\mathcal{T}_{m\mathbf{k}}$ reduce to matrices of 3×3 elements at each order $\epsilon^m\delta^n$. Likewise, the nonlinearity $\tilde{\mathbf{N}}_{m\mathbf{k}}$ reduces to a 3-component vector at each order $\epsilon^m\delta^n$.

At $\mathcal{O}(\epsilon^0\delta^0)$,

$$\mathcal{L}_{00,\mathbf{k}}\tilde{\mathbf{v}}_{00,\mathbf{k}} = \mathbf{0}, \quad (\text{B.1})$$

where

$$\mathcal{L}_{00,\mathbf{k}} = \begin{bmatrix} -\bar{S}\partial_z & \Omega D_{\mathbf{k}}^2 & -1 \\ 0 & \Omega D_{\mathbf{k}}^2 & -\Omega \\ 0 & -Q_{00}(k)k^2 & D_{\mathbf{k}}^2 \end{bmatrix}, \quad (\text{B.2})$$

with $D_{\mathbf{k}}^2 = \partial_z^2 - k^2$.

At $\mathcal{O}(\epsilon^0\delta^1)$,

$$\mathcal{L}_{00,\mathbf{k}}\tilde{\mathbf{v}}_{01,\mathbf{k}} = -\mathcal{L}_{01,\mathbf{k}}\tilde{\mathbf{v}}_{00,\mathbf{k}}, \quad (\text{B.3})$$

where

$$\mathcal{L}_{01,\mathbf{k}} = \begin{bmatrix} 0 & \Omega \partial_z & \Omega(z-1/2) \\ -\bar{S}/\bar{C}((z-1)\partial_z + 1) & \Omega^2 \partial_z & \Omega^2(z-1/2) \\ 0 & -Q_{01}(k)k^2 & 0 \end{bmatrix}. \quad (\text{B.4})$$

At $O(\epsilon^1 \delta^0)$,

$$\mathcal{L}_{00,\mathbf{k}} \tilde{\mathbf{v}}_{10,\mathbf{k}} = \tilde{\mathbf{N}}_{10,\mathbf{k}} - \mathcal{L}_{10,\mathbf{k}} \tilde{\mathbf{v}}_{00,\mathbf{k}}, \quad (\text{B.5})$$

where

$$\mathcal{L}_{10,\mathbf{k}} = \begin{bmatrix} 0 & 0 & 0 \\ 0 & 0 & 0 \\ 0 & -Q_{10}(k)k^2 & 0 \end{bmatrix}, \quad \tilde{\mathbf{N}}_{10,\mathbf{k}} = \int_{\mathbf{k}=\mathbf{p}+\mathbf{q}} \mathbf{d}\mathbf{p} \mathbf{d}\mathbf{q} \begin{bmatrix} \tilde{\mathbf{u}}_{00,\mathbf{p}} \cdot \mathbf{D}_{\mathbf{q}} \tilde{\theta}_{00,\mathbf{q}} \\ \Omega \tilde{\mathbf{u}}_{00,\mathbf{p}} \cdot \mathbf{D}_{\mathbf{q}} \tilde{\theta}_{00,\mathbf{q}} \\ 0 \end{bmatrix}, \quad (\text{B.6a,b})$$

in which $\mathbf{D}_{\mathbf{q}} = \hat{\mathbf{z}}\partial_z + \mathbf{i}\mathbf{q}$.

At $O(\epsilon^2 \delta^{-1})$:

$$\mathcal{L}_{00,\mathbf{k}} \tilde{\mathbf{v}}_{2,-1,\mathbf{k}} = -\mathcal{T}_{0,-1,\mathbf{k}} \partial_T \tilde{\mathbf{v}}_{00,\mathbf{k}}, \quad (\text{B.7})$$

where

$$\mathcal{T}_{0,-1,\mathbf{k}} = \begin{bmatrix} \bar{S} & 0 & 0 \\ 0 & 0 & 0 \\ 0 & 0 & 0 \end{bmatrix}. \quad (\text{B.8})$$

At $O(\epsilon^2 \delta^0)$:

$$\begin{aligned} \mathcal{L}_{00,\mathbf{k}} \tilde{\mathbf{v}}_{20,\mathbf{k}} &= \tilde{\mathbf{N}}_{20,\mathbf{k}} - \mathcal{L}_{01,\mathbf{k}} \tilde{\mathbf{v}}_{2,-1,\mathbf{k}} - \mathcal{L}_{10,\mathbf{k}} \tilde{\mathbf{v}}_{10,\mathbf{k}} - \mathcal{L}_{20,\mathbf{k}} \tilde{\mathbf{v}}_{00,\mathbf{k}} \\ &\quad - \mathcal{T}_{0,-1,\mathbf{k}} \partial_T \tilde{\mathbf{v}}_{01,\mathbf{k}} - \mathcal{T}_{00,\mathbf{k}} \partial_T \tilde{\mathbf{v}}_{00,\mathbf{k}}, \end{aligned} \quad (\text{B.9})$$

where

$$\mathcal{L}_{20,\mathbf{k}} = \begin{bmatrix} 0 & 0 & 0 \\ 0 & 0 & 0 \\ 0 & -Q_{20}(k)k^2 & 0 \end{bmatrix}, \quad \mathcal{T}_{00,\mathbf{k}} = \begin{bmatrix} 0 & -\Omega & 0 \\ \bar{S}/\bar{C}(z-1) & -\Omega^2 & 0 \\ 0 & 0 & 0 \end{bmatrix} \quad (\text{B.10a,b})$$

and

$$\begin{aligned} \tilde{\mathbf{N}}_{20,\mathbf{k}} &= \int_{\mathbf{k}=\mathbf{p}+\mathbf{q}} \mathbf{d}\mathbf{p} \mathbf{d}\mathbf{q} \begin{bmatrix} (\tilde{\mathbf{u}}_{10,\mathbf{p}} \cdot \mathbf{D}_{\mathbf{q}} \tilde{\theta}_{00,\mathbf{q}} + \tilde{\mathbf{u}}_{00,\mathbf{p}} \cdot \mathbf{D}_{\mathbf{q}} \tilde{\theta}_{10,\mathbf{q}}) \\ \Omega (\tilde{\mathbf{u}}_{10,\mathbf{p}} \cdot \mathbf{D}_{\mathbf{q}} \tilde{\theta}_{00,\mathbf{q}} + \tilde{\mathbf{u}}_{00,\mathbf{p}} \cdot \mathbf{D}_{\mathbf{q}} \tilde{\theta}_{10,\mathbf{q}}) \\ \bar{\mathcal{K}}_1/\Omega \{ \partial_z (\tilde{\mathbf{u}}_{00,\mathbf{p}} \cdot \mathbf{D}_{\mathbf{q}} \tilde{\phi}_{00,\mathbf{q}}) - \mathbf{D}_{\mathbf{k}}^2 (\tilde{w}_{00,\mathbf{p}} \tilde{\phi}_{00,\mathbf{q}}) \} \end{bmatrix} \\ &\quad + \frac{\mathcal{K}_2}{\Omega^2} \int_{\mathbf{k}=\mathbf{l}+\mathbf{m}+\mathbf{n}} \mathbf{d}\mathbf{l} \mathbf{d}\mathbf{m} \mathbf{d}\mathbf{n} \begin{bmatrix} 0 \\ 0 \\ \partial_z (\tilde{\mathbf{u}}_{00,\mathbf{l}} \cdot \mathbf{D}_{\mathbf{k}-1} (\tilde{\phi}_{00,\mathbf{m}} \tilde{\phi}_{00,\mathbf{n}})) \\ -\mathbf{D}_{\mathbf{k}}^2 (\tilde{w}_{00,\mathbf{l}} \tilde{\phi}_{00,\mathbf{m}} \tilde{\phi}_{00,\mathbf{n}}) \end{bmatrix}, \end{aligned} \quad (\text{B.10c})$$

where $\mathbf{D}_{\mathbf{p}} = \hat{\mathbf{z}}\partial_z + \mathbf{i}\mathbf{p}$ and $\mathbf{D}_{\mathbf{p}}^2 = |\mathbf{D}_{\mathbf{p}}|^2 = \partial_z^2 - p^2$.

Appendix C: Derivation of the pattern equation

In this appendix we provide some details of the derivation of the pattern equation (44) from the solvability condition for the $O(\epsilon^2\delta^0)$ equations (43). It is easy to see that the equation proportional to $\phi_{20\mathbf{k}}$ decouples from the rest of the system of ordinary differential equations so that we are left with

$$\Omega D_{\mathbf{k}}^2 \theta_{20\mathbf{k}} - \Omega w_{20\mathbf{k}} = N_{20\mathbf{k}}^\theta + \bar{S}/\bar{C} \phi_{2,-1\mathbf{k}} + \Omega^2 \partial_T \theta_{00\mathbf{k}}, \quad (\text{C.1a})$$

$$D_{\mathbf{k}}^2 w_{20\mathbf{k}} - Q_{00}(\mathbf{k}) k^2 \theta_{20\mathbf{k}} = N_{20\mathbf{k}}^w + Q_{20}(\mathbf{k}) k^2 \theta_{00\mathbf{k}}, \quad (\text{C.1b})$$

where we have made use of (41) and $N_{20\mathbf{k}}^\theta$ and $N_{20\mathbf{k}}^w$ are given by (B.10c).

The solvability condition (35) for this system of inhomogeneous ordinary differential equations gives

$$\mathcal{I}_1 + \mathcal{I}_2 + \mathcal{I}_3 = 0, \quad (\text{C.2a})$$

in which

$$\mathcal{I}_1 = \int_0^1 dz \sin(\pi z) \left(\frac{\bar{S}}{\bar{C}} \phi_{2,-1\mathbf{k}} + \Omega^2 \partial_T \theta_{00\mathbf{k}} \right), \quad (\text{C.2b})$$

$$\mathcal{I}_2 = -\Omega \frac{Q_{20} k^2}{\pi^2 + k^2} \int_0^1 dz \sin(\pi z) \theta_{00\mathbf{k}}, \quad (\text{C.2c})$$

$$\mathcal{I}_3 = \int_0^1 dz \sin(\pi z) \left(N_{20\mathbf{k}}^\theta - \frac{\Omega}{\pi^2 + k^2} N_{20\mathbf{k}}^w \right). \quad (\text{C.2d})$$

Making use of expression (42) for $\phi_{2,-1\mathbf{k}}$, the integral \mathcal{I}_1 is evaluated as

$$\mathcal{I}_1 = -\frac{\Omega}{2} \lambda_{\mathbf{k}} \partial_T \tilde{f}_{\mathbf{k}}, \quad \text{where } \lambda_{\mathbf{k}} = \Omega - \frac{\pi^2 + k^2}{\pi^2} \frac{\bar{S}}{\Omega \bar{C}}. \quad (\text{C.3a})$$

Likewise, the integral \mathcal{I}_2 is evaluated using expression (30) for $\theta_{00\mathbf{k}}$ to give

$$\mathcal{I}_2 = \frac{\Omega}{2} \frac{Q_{20} k^2}{\pi^2 + k^2} \tilde{f}_{\mathbf{k}}. \quad (\text{C.3b})$$

Finally, we split the integral \mathcal{I}_3 into a quadratic and a cubic term so that

$$\mathcal{I}_3 = \frac{\Omega}{2} (M_{\mathbf{k}} - N_{\mathbf{k}}), \quad (\text{C.3c})$$

where

$$\begin{aligned} M_{\mathbf{k}} \{\tilde{f}^2\} &= -\frac{\bar{K}_1}{\Omega(\pi^2 + k^2)} \int_{\mathbf{k}=\mathbf{p}+\mathbf{q}} d\mathbf{p} d\mathbf{q} \int_0^1 dz \sin(\pi z) \\ &\quad \times \left(\partial_z (\tilde{\mathbf{u}}_{00,\mathbf{p}} \cdot \mathbf{D}_{\mathbf{q}} \tilde{\phi}_{00,\mathbf{q}}) - D_{\mathbf{k}}^2 (\tilde{w}_{00,\mathbf{p}} \tilde{\phi}_{00,\mathbf{q}}) + (p \leftrightarrow q) \right), \end{aligned} \quad (\text{C.4a})$$

$$\begin{aligned}
N_{\mathbf{k}}\{\tilde{f}^3\} &= \frac{2K_2}{\Omega^2(\pi^2 + k^2)} \int_{\mathbf{k}=\mathbf{l}+\mathbf{m}+\mathbf{n}} d\mathbf{l} d\mathbf{m} d\mathbf{n} \int_0^1 dz \sin(\pi z) \\
&\quad \times \left\{ \partial_z (\mathbf{u}_{00\mathbf{l}} \cdot \mathbf{D}_{\mathbf{k}-\mathbf{l}}(\phi_{00\mathbf{m}}\phi_{00\mathbf{n}})) - D_{\mathbf{k}}^2(w_{00\mathbf{l}}\phi_{00\mathbf{m}}\phi_{00\mathbf{n}}) \right\} \\
&\quad - 2 \int_{\mathbf{k}=\mathbf{l}+\mathbf{m}+\mathbf{n}} d\mathbf{l} d\mathbf{m} d\mathbf{n} \int_0^1 dz \sin(\pi z) \\
&\quad \times (\mathbf{u}_{10\mathbf{m}+\mathbf{n}} \cdot \mathbf{D}_1\theta_{00\mathbf{l}} + \mathbf{u}_{00\mathbf{l}} \cdot \mathbf{D}_{\mathbf{m}+\mathbf{n}}\theta_{10\mathbf{m}+\mathbf{n}}). \tag{C.4b}
\end{aligned}$$

Making use of expressions for the $O(\epsilon^0\delta^0)$ and $O(\epsilon^1\delta^0)$ variables and evaluating the integrals over z , it is straightforward (if tedious) to show that (C.4a,b) reduce to

$$M_{\mathbf{k}}\{\tilde{f}^2\} \equiv \int_{\mathbf{k}=\mathbf{p}+\mathbf{q}} d\mathbf{p} d\mathbf{q} \mathcal{M}_{\mathbf{pq}}^{\mathbf{k}} \tilde{f}_{\mathbf{p}} \tilde{f}_{\mathbf{q}}, \tag{C.5a}$$

$$N_{\mathbf{k}}\{\tilde{f}^3\} \equiv \frac{1}{3} \int_{\mathbf{k}=\mathbf{l}+\mathbf{m}+\mathbf{n}} d\mathbf{l} d\mathbf{m} d\mathbf{n} \left(\mathcal{N}_{\mathbf{lmm}}^{\mathbf{k}} + \mathcal{N}_{\mathbf{nml}}^{\mathbf{k}} + \mathcal{N}_{\mathbf{mnl}}^{\mathbf{k}} \right) \tilde{f}_{\mathbf{l}} \tilde{f}_{\mathbf{m}} \tilde{f}_{\mathbf{n}}, \tag{C.5b}$$

with

$$\mathcal{M}_{\mathbf{pq}}^{\mathbf{k}} = \mathcal{M}_{\mathbf{qp}}^{\mathbf{k}} = \frac{2\pi\bar{K}_1}{\bar{C} + \bar{S}} \frac{(\pi^2 + p^2)(\pi^2 + q^2)}{(\pi^2 + k^2)} \left\{ \frac{\mathbf{p} \cdot \mathbf{q}}{2} \left(\frac{1}{p^2} + \frac{1}{q^2} \right) + \frac{\pi^2 + k^2}{\pi^2} \right\}, \tag{C.6a}$$

and

$$\begin{aligned}
\mathcal{N}_{\mathbf{lmm}}^{\mathbf{k}} = \mathcal{N}_{\mathbf{lmm}}^{\mathbf{k}} &= \frac{K_2}{4(\bar{C} + \bar{S})^2} \frac{(\pi^2 + l^2)(\pi^2 + m^2)(\pi^2 + n^2)}{(\pi^2 + k^2)} \left(\frac{5k^2}{\pi^2} + \frac{7\mathbf{k} \cdot \mathbf{l}}{l^2} \right) \\
&\quad + \frac{1}{24} \frac{\pi^2 + |\mathbf{m} + \mathbf{n}|^2}{5\pi^2 + 2|\mathbf{m} + \mathbf{n}|^2} \left\{ (\pi^2 + |\mathbf{m} + \mathbf{n}|^2) \frac{k^2 - l^2}{|\mathbf{k} - \mathbf{l}|^2} - (\pi^2 + l^2) \frac{4\pi^2 + |\mathbf{m} + \mathbf{n}|^2}{\pi^2 + |\mathbf{m} + \mathbf{n}|^2} \left(1 + \frac{\mathbf{k} \cdot \mathbf{l}}{l^2} \right) \right\} \\
&\quad \times \left\{ (\pi^2 + m^2) \left(\frac{\mathbf{m} \cdot \mathbf{n}}{m^2} - 1 \right) + (\pi^2 + n^2) \left(\frac{\mathbf{m} \cdot \mathbf{n}}{n^2} - 1 \right) \right\}. \tag{C.6b}
\end{aligned}$$

It can be shown, using the relation $\mathbf{k} = \mathbf{p} + \mathbf{q}$, that the kernel $\mathcal{M}_{\mathbf{pq}}^{\mathbf{k}}$ is positive and vanishes only when $|\mathbf{k}| = 0$.

We now evaluate the integrals $M_{\mathbf{k}}\{\tilde{f}^2\}$ and $N_{\mathbf{k}}\{\tilde{f}^3\}$ under the assume that $\tilde{f}_{\mathbf{p}} = F(\alpha_{\mathbf{p}})\pi^{-1}\delta(|\mathbf{p}| - k_c)$, where $\alpha_{\mathbf{p}}$ is the angle \mathbf{p} makes with $\mathbf{k} = k\hat{\mathbf{x}}$. In this case, the constraint $\mathbf{k} = \mathbf{p} + \mathbf{q}$ implies that

$$\mathbf{p} \cdot \mathbf{q} = (k^2 - p^2 - q^2)/2 = -\pi^2/2, \tag{C.7}$$

so that $M_{\mathbf{k}}$ can be straightforwardly evaluated to give

$$M_{\mathbf{k}} = 3\pi^2 \frac{\bar{K}_1}{\bar{C} + \bar{S}} \int_{\mathbf{k}=\mathbf{p}+\mathbf{q}} d\alpha_p d\alpha_q F(\alpha_p) F(\alpha_q). \tag{C.8}$$

Without loss of generality we set $\alpha_k = 0$ so that $\mathbf{k} = k_c\hat{\mathbf{x}}$. We note that there are two possible orientations of \mathbf{p}, \mathbf{q} satisfying $\mathbf{k} = \mathbf{p} + \mathbf{q}$ when $p = q = \pi$: (a) $\alpha_p = \pi/3, \alpha_q = -\pi/3$, and (b) $\alpha_p = -\pi/3, \alpha_q = \pi/3$. As both these make the same contribution to $M_{\mathbf{k}}$ we have

$$M_{\mathbf{k}} = 6\pi^2 \frac{\bar{K}_1}{\bar{C} + \bar{S}} F\left(+\frac{\pi}{3}\right) F\left(-\frac{\pi}{3}\right). \tag{C.9}$$

To evaluate the cubic nonlinearity $N_{\mathbf{k}}$ we note that the constraints $\mathbf{k} = \mathbf{l} + \mathbf{m} + \mathbf{n}$ and $k = l = m = n = \pi$ are simultaneously satisfied in three cases (Ma 2009):

$$(i) \mathbf{k} = \mathbf{l}, \mathbf{m} = -\mathbf{n}, \quad (ii) \mathbf{k} = \mathbf{m}, \mathbf{l} = -\mathbf{n}, \quad (iii) \mathbf{k} = \mathbf{n}, \mathbf{l} = -\mathbf{m}.$$

Cases (ii) and (iii) are the same, because of the symmetry of the kernel $\mathcal{N}_{\mathbf{lmn}}^{\mathbf{k}}$ under $\mathbf{m} \leftrightarrow \mathbf{n}$ which leads to

$$\mathcal{N}_{\mathbf{lmn}}^{\mathbf{k}(ii)} = \mathcal{N}_{\mathbf{lmn}}^{\mathbf{k}(iii)} = \pi^4 \frac{\mathcal{K}_2}{(\bar{C} + \bar{S})^2} (5 + 7 \cos \alpha) + \frac{2\pi^4}{3} (1 + \cos \alpha)^2 \frac{3 - \cos \alpha}{9 - 4 \cos \alpha}, \quad (C.10)$$

where we have made use of $\mathbf{k} \cdot \mathbf{l} = -\mathbf{m} \cdot \mathbf{n} = \pi^2 \cos \alpha$.

Case (i) possesses a term proportional to $(k^2 - l^2)/|\mathbf{k} - \mathbf{l}|^2$, which is singular in the limit $\mathbf{k} = \mathbf{l}$. To evaluate $\mathcal{N}_{\mathbf{lmn}}^{\mathbf{k}(i)}$, we follow the approach of Ma (2009) and assume that $\tilde{f}_{\mathbf{k}}$ has support in a small but nonzero band of wavenumbers such that $\mathbf{k} = \mathbf{k}_0 + \mathbf{k}_1$, etc., and

$$\mathbf{k}_0 = \mathbf{l}_0, \quad \mathbf{m}_0 = -\mathbf{n}_0, \quad \mathbf{k}_1 = \mathbf{l}_1 + \mathbf{m}_1 + \mathbf{n}_1. \quad (C.11)$$

Taking $\mathbf{k}_0 = k_c \hat{\mathbf{x}}$ and $\mathbf{k}_1 - \mathbf{l}_1 = k'(\cos \alpha' \hat{\mathbf{x}} + \sin \alpha' \hat{\mathbf{y}})$ (with $k' \ll k_c$) we find that

$$\frac{k^2 - l^2}{|\mathbf{k} - \mathbf{l}|^2} = \frac{2k_c \cos \alpha'}{k'} + \frac{k_1^2 - l_1^2}{k'^2}. \quad (C.12)$$

By averaging this over $(\mathbf{k}_1, \mathbf{l}_1, \mathbf{m}_1, \mathbf{n}_1)$ at fixed $(\mathbf{k}_0, \mathbf{l}_0, \mathbf{m}_0, \mathbf{n}_0)$, we find that the first term in this expression is proportional to

$$\left\langle \frac{k_c \cos \alpha'}{k'} \right\rangle = 0, \quad (C.13)$$

while the second term is proportional to

$$\langle k_1^2 \rangle - \langle l_1^2 \rangle = 0, \quad (C.14)$$

by symmetry. Thus, the term $(k^2 - l^2)/|\mathbf{k} - \mathbf{l}|^2$ vanishes and we find that

$$\mathcal{N}_{\mathbf{lmn}}^{\mathbf{k}(i)} = 12\pi^4 \frac{\mathcal{K}_2}{(\bar{C} + \bar{S})^2} + \frac{16\pi^4}{15}. \quad (C.15)$$

Combining these results we find that

$$\mathcal{N}_{\mathbf{k}} = \int_{\mathbf{k}=\mathbf{l}+\mathbf{m}+\mathbf{n}} d\alpha_l d\alpha_m d\alpha_n F(\alpha_l) F(\alpha_m) F(\alpha_n) \left(\mathcal{N}_{\mathbf{lmn}}^{\mathbf{k}(i)} + \mathcal{N}_{\mathbf{lmn}}^{\mathbf{k}(ii)} + \mathcal{N}_{\mathbf{lmn}}^{\mathbf{k}(iii)} \right). \quad (C.16)$$

Finally, we note that $\alpha_l, \alpha_m, \alpha_n$ can take values that are cyclic permutations of 0, α and $\alpha - \pi$ so that

$$\begin{aligned} \mathcal{N}_{\mathbf{k}} &= \frac{8\pi^6}{3} \int_0^{2\pi} d\alpha F(0) F(\alpha) F(\alpha - \pi) \\ &\quad \times \left\{ \frac{3\mathcal{K}_2}{2(\bar{C} + \bar{S})^2} (11 + 7 \cos \alpha) + (1 + \cos \alpha)^2 \frac{3 - \cos \alpha}{9 - 4 \cos \alpha} \right\}. \end{aligned} \quad (C.17)$$

Note that this expression is strictly positive.